J|A|C|S
ARTICLES

Published on Web 03/10/2010

Tri-N-annulated Hexarylene: An Approach to Well-Defined Graphene Nanoribbons with Large Dipoles

Yan Li,[†,‡] Jing Gao,[†,‡] Simone Di Motta,[§] Fabrizia Negri,*[,§] and Zhaohui Wang*[,†]

Beijing National Laboratory for Molecular Sciences, Institute of Chemistry, Chinese Academy of Sciences, Beijing 100190, People's Republic of China, Graduate School of the Chinese Academy of Sciences, Beijing 100190, People's Republic of China, Dipartimento di Chimica "G. Ciamician", Università di Bologna, Via F. Selmi 2, 40126 Bologna, Italy, and INSTM, UdR Bologna, Italy

Received October 14, 2009; E-mail: wangzhaohui@iccas.ac.cn; fabrizia.negri@unibo.it

Abstract: We report a highly efficient synthetic methodology toward tri-N-annulated hexarylenes from easily available N-annulated perylenes, which is favored by the oxidative ring fusion driven by DDQ/$Sc(OTf)_3$. To assist the characterization of the new compounds, quantum-chemical calculations of structural and spectroscopic properties have been carried out for three oligomers of N-annulated rylenes. It is shown that tri-N-annulated hexarylene dyes display remarkably large dipole moments likely associated with the formation of H aggregates, as suggested by the marked concentration dependence of the measured UV−vis spectra. It is suggested that the combination of $\pi-\pi$ stacking interactions and dipole−dipole interactions may favor the formation of highly ordered supramolecular structures, resulting in enhanced charge carrier mobilities.

Introduction

Graphene nanoribbons (GNRs), in which the lateral quantum confinement opens an electronic gap that is a function of the ribbon width, have opened the way to a breakthrough in carbon-based nanoelectronics.[1] Driven by these, a great effort has been devoted to developing methods for the preparation of graphene nanoribbons. Lithographic patterning of graphene sheets has led to the fabrication of GNRs down to widths of ~20 nm thus far,[2] but there have been difficulties in obtaining smooth edges and reaching true nanometer-scale ribbon width. Quite recently, Dai and Tour have reported respectively simple and inexpensive methods to prepare GNRs with defined shape by the longitudinal unzipping of multiwalled carbon nanotubes (MWCNTs).[3] Dresselhaus demonstrated an efficient shaping of defective rough graphitic nanoribbon edges into atomically smooth zigzag or armchair edges via Joule heating inside a TEM-STM system.[4] As for functionalized graphene nanoribbons (F-GNRs), it is promising that edge doping by nitrogen species can transform p-type GNRs into n-type transistors.[5] On the other hand, Müllen also reported a new synthetic approach to linear F-GNRs with branched alkyl chains exhibiting good solubility and length up to 12 nm, which was never achieved before.[6] As GNRs consist of infinite repeating polycyclic aromatic units in one dimension, which can be easily decorated, the bottom-up organic synthetic methodologies can be regarded as the most promising way to functionalized graphene nanoribbons (F-GNRs).

The copper-mediated condensation of perylene-3,4:9,10-tetracarboxylic acid bis-imides (PBIs) along the bay region (short molecular axis) was used to construct graphene-type nanoribbons that are functionalized by arrays of imide groups (Figure 1, **1**).[7] However, due to the two possible coupling positions, there are structural isomers of oligo-PBIs, which hinder further attempts toward the effective synthesis of higher homologues and structurally perfect poly(bay-PBIs).[8]

While the intriguing structural and electro-optical properties of poly(*peri*-naphthalene) (PPN) have led to the pursuit of its rational synthesis, to date, hexarylene[9] and the higher homologues remain elusive targets for chemists due to the lack of suitable building blocks and effective synthetic methods for the long-range extension of π conjugation as well as their impro-

[†] Beijing National Laboratory for Molecular Sciences.
[‡] Graduate School of the Chinese Academy of Sciences.
[§] Università di Bologna and INSTM.

(1) (a) Novoselov, K. S.; Geim, A. K.; Morozov, S. V.; Jiang, D.; Zhang, Y.; Dubonos, S. V.; Grigorieva, I. V.; Firsov, A. A. *Science* **2004**, *306*, 666–669. (b) Geim, A. K.; Novoselov, K. S. *Nat. Mater.* **2007**, *6*, 183–191. (c) Li, X.; Wang, X.; Zhang, L.; Lee, S.; Dai, H. *Science* **2008**, *319*, 1229–1232. (d) Wang, X.; Ouyang, Y.; Li, X.; Wang, H.; Guo, J.; Dai, H. *Phys. Rev. Lett.* **2008**, *100*, 206803.
(2) Han, M. Y.; Özyilmaz, B.; Zhang, Y.; Kim, P. *Phys. Rev. Lett.* **2007**, *98*, 206805.
(3) (a) Jiao, L.; Zhang, L.; Wang, X.; Diankov, G.; Dai, H. *Nature* **2009**, *458*, 877–880. (b) Kosynkin, D. V.; Higginbotham, A. L.; Sinitskii, A.; Lomeda, J. R.; Dimiev, A.; Price, B. K.; Tour, J. M. *Nature* **2009**, *458*, 872–876.
(4) Jia, X.; Hofmann, M.; Meunier, V.; Sumpter, B. G.; Campos-Delgado, J.; Romo-Herrera, J. M.; Son, H.; Hsieh, Y. P.; Reina, A.; Kong, J.; Terrones, M.; Dresselhaus, M. S. *Science* **2009**, *323*, 1701–1705.
(5) (a) Wang, X.; Li, X.; Zhang, L.; Yoon, Y.; Weber, P. K.; Wang, H.; Guo, J.; Dai, H. *Science* **2009**, *324*, 768–771. (b) Yan, Q.; Huang, B.; Yu, J.; Zheng, F.; Zang, J.; Wu, J.; Gu, B. L.; Liu, F.; Duan, W. *Nano Lett.* **2007**, *7*, 1469–1473.
(6) Yang, X.; Dou, X.; Rouhanipour, A.; Zhi, L.; Räder, H. J.; Müllen, K. *J. Am. Chem. Soc.* **2008**, *130*, 4216–4217.
(7) Qian, H.; Wang, Z.; Yue, W.; Zhu, D. *J. Am. Chem. Soc.* **2007**, *129*, 10664–10665.
(8) Qian, H.; Negri, F.; Wang, C.; Wang, Z. *J. Am. Chem. Soc.* **2008**, *130*, 17970–17976.
(9) Hexarylene bis(dicarboximide) was reported by Müllen: Pschirer, N. G.; Kohl, C.; Nolde, F.; Qu, J.; Müllen, K. *Angew. Chem., Int. Ed. Engl.* **2006**, *45*, 1401–1404.

 10.1021/ja100276x © **2010 American Chemical Society**

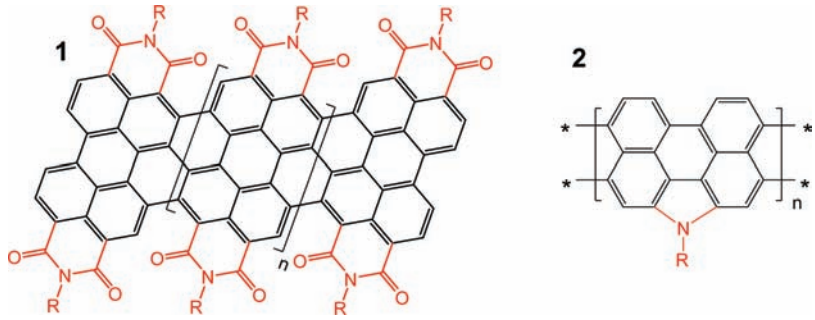

Figure 1. Poly(bay-PBIs) **1** and poly(*peri*-N-annulated-perylenes) **2**.

cessability caused by their poor solubility.[10] Recently we reported the one-pot synthesis of bis-N-annulated quaterrylene (BNQ, **16**) based on the practical synthesis of a new building block, N-annulated perylene (NP).[11] Poly(*peri*-N-annulated-perylene) (PPNP) can be regarded as perfect graphene ribbons incorporating nitrogen atoms into the armchair edge structures, providing ideal model compounds for chemically modified graphene ribbons with large dipoles. In this contribution, we present tri-N-annulated hexarylenes containing three space-demanding, branched alkyl chains and a variety of end-cap pending groups to guarantee their good processability, which represent a new approach toward the rational synthesis of graphene nanoribbons with well-defined edges. Tri-N-annulated hexarylenes have been characterized both experimentally and computationally. Electric and electronic properties have been determined, and evidence for the formation of H aggregates has been provided by comparing measured and computed absorption spectra.

Computational Details

The chosen models for N-annulated rylenes did not include the naphthyl substituents, since these contribute negligibly to the final structural and electronic properties of the extended conjugated chromophores. Atomic structures were optimized with density functional theory (DFT) calculations using the B3LYP hybrid functional[12] with the basis set limited to 3-21G owing to the large dimension of the chromophores. The small basis set results were validated with additional calculations carried out with the 6-31G* basis set. Molecular orbital shapes and energies discussed in the text are those calculated at the optimized structures. Orbital pictures were prepared with Molekel 4.3 visual software.[13] Electronic excitation energies and oscillatior strengths were computed with time-dependent (TD) DFT calculations. In plotting computed electronic spectra, a Lorentzian line width of 0.1 eV was superimposed on each computed intensity to facilitate the comparison with experimental spectra. The Franck−Condon (FC) vibronic structure[14] associated with electronic transitions was evaluated along the lines described in previous work[15] and as detailed in the Supporting Information. To model the possible aggregates, we considered a dimer and a trimer maximizing the dipole−dipole interaction, with molecules at a distance of 3.5 Å. It is interesting to note that the orientation determined by the attractive dipole−dipole interaction implies a parallel orientation of the transition dipole moments, which is typical for H aggregates. All quantum-chemical calculations were performed with the Gaussian03 package.[16]

Synthesis and Characterization

The synthesis is shown in Scheme 1. Regioselective NBS bromination of NP with dovetailed alkyl substituents provided the key building blocks, denoted monobrominated NP (**3**) and dibrominated alkylated NP (**12**), for the construction of N-modified GNRs. Suzuki−Miyaura coupling of **3** and arylboronic acid afford mono-end-capped NP, which can be further selectively brominated to **9**−**11.** Compound **12** was converted to the diboronate **13** via bromine−lithium exchange followed by reaction of the lithium intermediate with 2-isopropoxy-4,4,5,5-tetramethyl-1,3,2-dioxaborolane. Subsequently, Suzuki−Miyaura coupling of **9**−**11** with **13** affords the key precursor **14** for the final ring fusion. When **14** was treated with 5 equiv of 2,3-dichloro-5,6-dicyano-1,4-benzoquinone (DDQ) and scandium trifluoromethanesulfonate ($Sc(OTf)_3$) in toluene at 110 °C for 24 h, the expansion of the π system was successfully achieved along the long molecular axis to afford tri-N-annulated hexarylenes (TNH) **15** in 61−73% yield. For comparison, bis-N-annulated quaterrylene was prepared according to the known procedure.[11a] Although the use of DDQ/$Sc(OTf)_3$ has been proven to be powerful in the extension of electron-rich π-conjugated systems to prepare triply linked oligoporphyrins,[17] there are only a few examples of the more accessible polycyclic aromatics.[18] It is remarkable that, under this simple condition, the expansion of the π system was successfully and highly effectively achieved along the long molecular axis, which opens a new avenue toward graphene ribbon-type molecules.

Electric and Electronic Properties of N-annulated Rylenes

The B3LYP/3-21G optimized geometries of NP, BNQ, and TNH are collected in Figure S1. It is seen that the extended

(10) (a) Brédas, J. L.; Baughman, R. H. *J. Chem. Phys.* **1985**, *83*, 1316. (b) Scherf, U.; Müllen, K. *Synthesis* **1992**, *1*−*2*, 23–38. (c) Koch, K.; Müllen, K. *Chem. Ber.* **1991**, *124*, 2091–2100. (d) Bohnen, A.; Koch, K.; Luettke, W.; Müllen, K. *Angew. Chem., Int. Ed. Engl.* **1990**, *29*, 525–527.
(11) (a) Li, Y.; Wang, Z. *Org. Lett.* **2009**, *11*, 1385–1387. (b) Jiang, W.; Qian, H.; Li, Y.; Wang, Z. *J. Org. Chem.* **2008**, *73*, 7369–7372.
(12) Becke, A. D. *J. Chem. Phys.* **1993**, *98*, 5648.
(13) Molekel Version 4.3, http://www.cscs.ch/molkel/: Portmann, S.; Lüthi, H. P. *Chimia* **2000**, *54*, 766.
(14) (a) Jankowiak, H. C.; Stuber, J. L.; Berger, R. *J. Chem. Phys.* **2007**, *127*, 234101. (b) Santoro, F.; Improta, R.; Lami, A.; Bloino, J.; Barone, V. *J. Chem. Phys.* **2007**, *126*, 084509. (c) Santoro, F.; Lami, A.; Improta, R.; Barone, V. *J. Chem. Phys.* **2007**, *126*, 184102. (d) Dierksen, M.; Grimme, S. *J. Chem. Phys.* **2004**, *120*, 3544–3554. (e) Borrelli, R.; Peluso, A. *J. Chem. Phys.* **2003**, *119*, 8437–8448.
(15) (a) Keszthelyi, T.; Balakrishnan, G.; Wilbrandt, R.; Yee, W. A.; Negri, F. *J. Phys. Chem. A* **2000**, *104*, 9121–9129. (b) Di Donato, E.; Vanzo, D.; Semeraro, M.; Credi, A.; Negri, F. *J. Phys. Chem. A* **2009**, *113*, 6504–6510.
(16) Gaussian 03, Revision C.02; Gaussian, Inc., Wallingford, CT, 2004.
(17) (a) Tsuda, A.; Osuka, A. *Science* **2001**, *293*, 79–82. (b) Hiroto, S.; Osuka, A. *J. Org. Chem.* **2005**, *70*, 4054–4058. (c) Tsuda, A.; Fruta, H.; Osuka, A. *Angew. Chem., Int. Ed.* **2000**, *39*, 2549–2552.
(18) Davis, N. K. S.; Pawlicki, M.; Anderson, H. L. *Org. Lett.* **2008**, *10*, 3945–3947.

Scheme 1. Synthesis of N-annulated Rylenes[a]

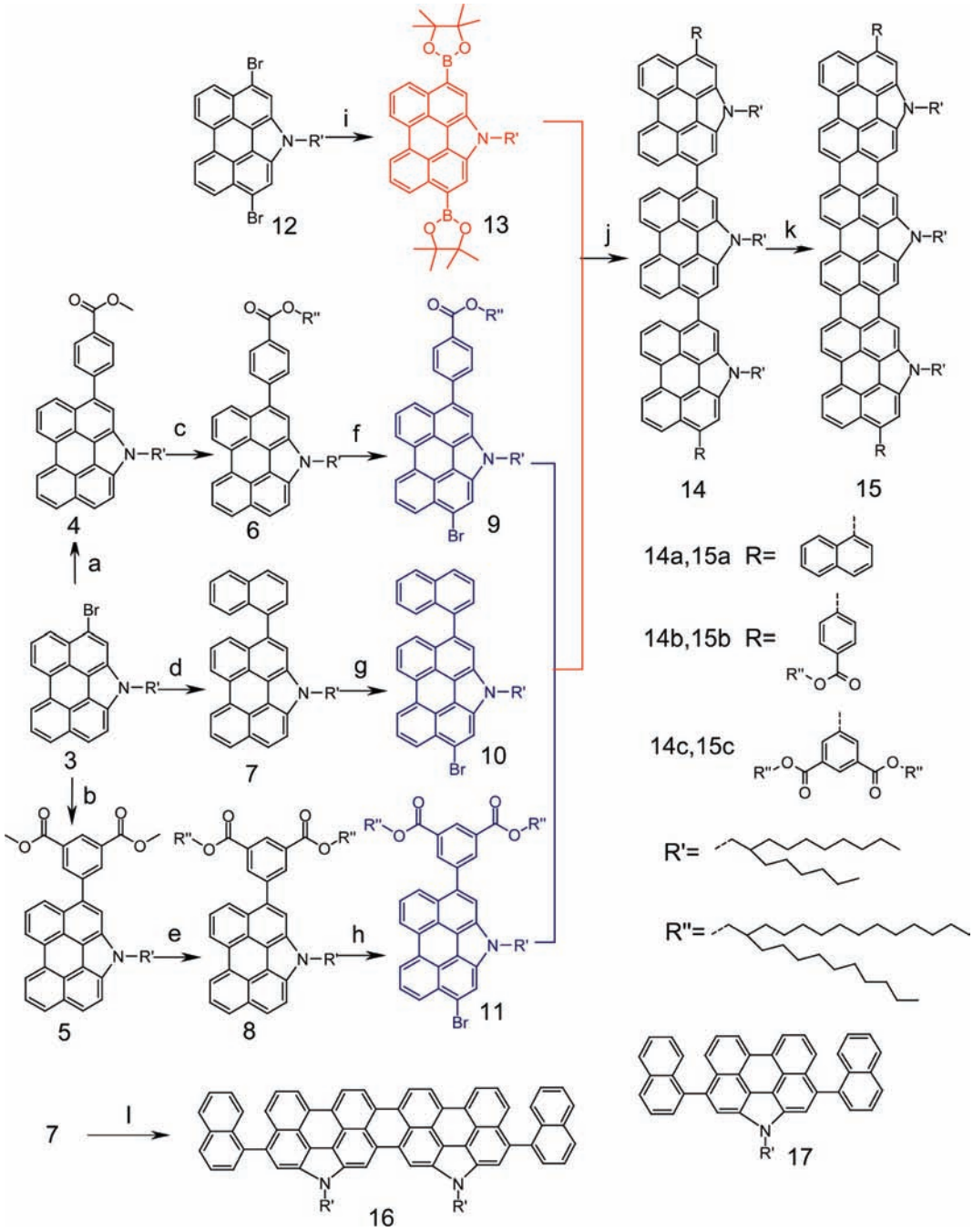

[a] Conditions: (a) 4-(methoxycarbonyl)benzeneboronic acid, $Pd(PPh_3)_4$, K_2CO_3, THF, 66 °C, 12 h, 87%; (b) 3,5-bis(methoxycarbonyl)benzeneboronic acid, $Pd(PPh_3)_4$, K_2CO_3, THF, 66 °C, 12 h, 83%; (c, e) (i) KOH, THF, 66 °C, 24 h, 98%, (ii) 2-decyl-1-tetradecanol, EDAC, DMAP, CH_2Cl_2, 25 °C, 12 h, 86% for **6**, 80% for **8**; (d) 1-naphthaleneboronic acid, $Pd(PPh_3)_4$, K_2CO_3, THF, 66 °C, 12 h, 90%; (f−h) NBS, CH_2Cl_2, 25 °C, 30 min, 96% for **9** and **11**, 92% for **10**; (i) *n*-BuLi, 2-isopropoxy-4,4,5,5-tetramethyl-1,3,2-dioxaborolane, THF, −78 °C, 12 h, 63%; (j) $Pd(PPh_3)_4$, K_2CO_3, THF, 66 °C, 18 h, 76% for **14a**, 72% for **14b** and **14c**; (k) $Sc(OTf)_3$, DDQ, toluene, 110 °C, 24 h, 73% for **15a**, 65% for **15b**, 61% for **15c**; (l) $Sc(OTf)_3$, DDQ, toluene, 50 °C, 24 h, 23%.

conjugation results in a large planar carbon skeleton. The computed bond length changes (bond numbering defined in Figure S2) upon excitation are collected in Figures S3 and S4. The computed dipole moments for the three systems, oriented along the short molecular axis as shown in Figure S1, are 2.69, 5.08, and 7.41 D. The remarkably large dipole moment of TNH may result in an increased ability to form aggregates. The frontier molecular orbitals in Figure 2 indicate a marked reduction of the electronic gap, consistent with the remarkable red shift of the absorption spectrum of TNH in comparison to NP and BNQ (see below). We note that the energy of the HOMO level increases remarkably, which may result in exceptional electron-donating properties of TNH.

Absorption Spectra

TNHs are dark green solids and are soluble in common organic solvents. Room-temperature absorption spectra of **17**, **16**, and **15a**−**c** in THF are shown in Figure 3. In sharp contrast, the spectrum of **15** displays a drastic bathochromic shift (403 nm, 173 nm) compared with those of NP (**17**) and BNQ (**16**),

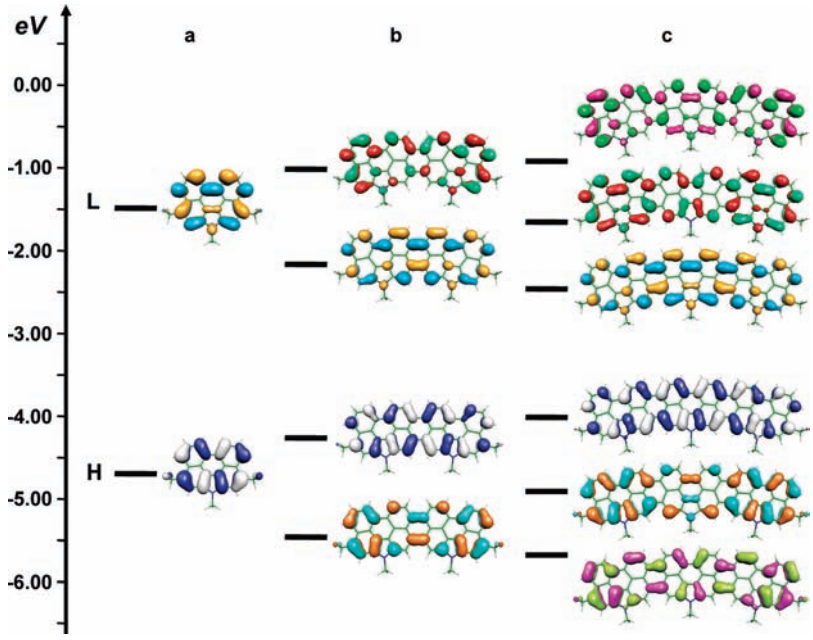

Figure 2. B3LYP/3-21G frontier molecular orbitals of (a) NP, (b) BNQ, and (c) TNH.

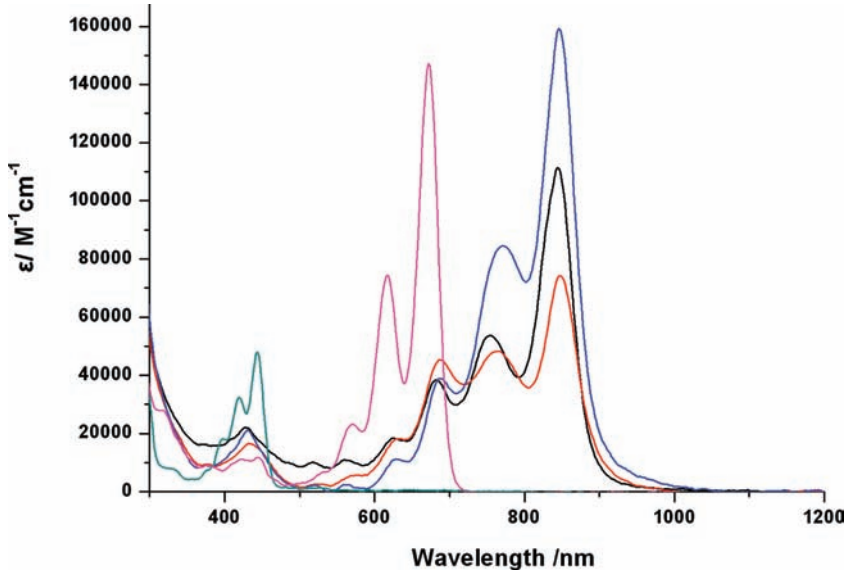

Figure 3. UV/vis absorption spectra of **17** (cyan), **16** (magenta), **15a** (black), **15b** (red), and **15c** (blue) in THF (1×10^{-6} M). The apparent reduction of ε for **15a**−**c** is due to the fact that only a fraction of the monomer is present, while the remaining TNH is present in the form of aggregate.

respectively, which reflects how the ladder-type conjugated structure leads to a great degree of planarity and correspondingly large delocalization of electronic wave functions with an absorption maximum at 846 nm. Interestingly, the introduction of sterically bulky end groups has a strong influence on the absorption coefficient as a reflection of the strong aggregation of **15** (see below).

The simulated vibronic spectra of NP and BNQ are compared with the experimental counterparts in Figure 4, from which it is clear that computed activities agree very nicely with the observed vibronic structure. On the basis of calculations we can formulate an assignment of the most prominent FC structure in the two spectra, which results in association with the normal coordinates shown in Figures S5 and S6. The peaks observed at 443, 418, 396, and 375 nm in the experimental absorption spectrum of NP correspond to a separation of ca. 1350 cm^{-1}. The observed peak separation is nicely reproduced by the simulated spectra, indicating the activity of a number of vibrations with frequencies ranging between 1238 and 1336 cm^{-1}. In addition, band shapes are modulated by the activity of a low-frequency mode at ca. 350 cm^{-1}, which describes an in-plane expansion of the whole molecule along its long molecular axis. For BNQ the most active vibration is computed at ca. 1250 cm^{-1}, but band shapes are modulated by the remarkably active vibration at 166 cm^{-1} in the acoustic phonon region, corresponding to the molecular expansion in the long molecular axis whose activity has been documented in other PAH systems.[19]

(19) Di Donato, E.; Tommasini, M.; Fustella, G.; Brambilla, L.; Castiglioni, C.; Zerbi, G.; Simpson, C. D.; Müllen, K.; Negri, F. *Chem. Phys.* **2004**, *301*, 81–93.

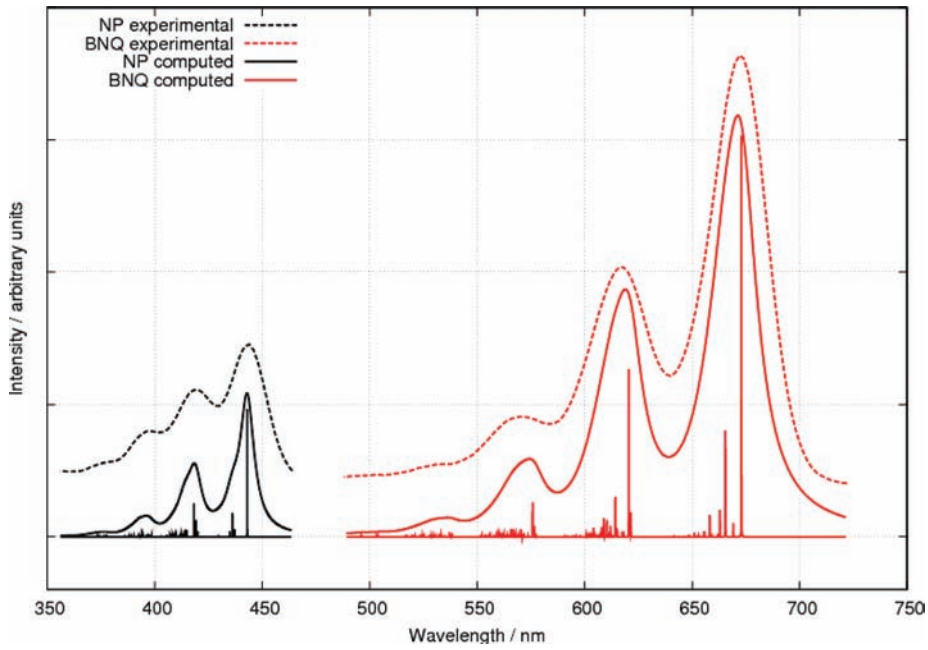

Figure 4. Comparison between observed (dashed) and computed (solid) spectra (including computed vibronic structure) for NP in black and BNQ in red. The fine structure shown under the broad computed spectra represents the FC activity contributions to each broad band. The origins of the computed spectra were translated to the origins of the respective experimental spectra.

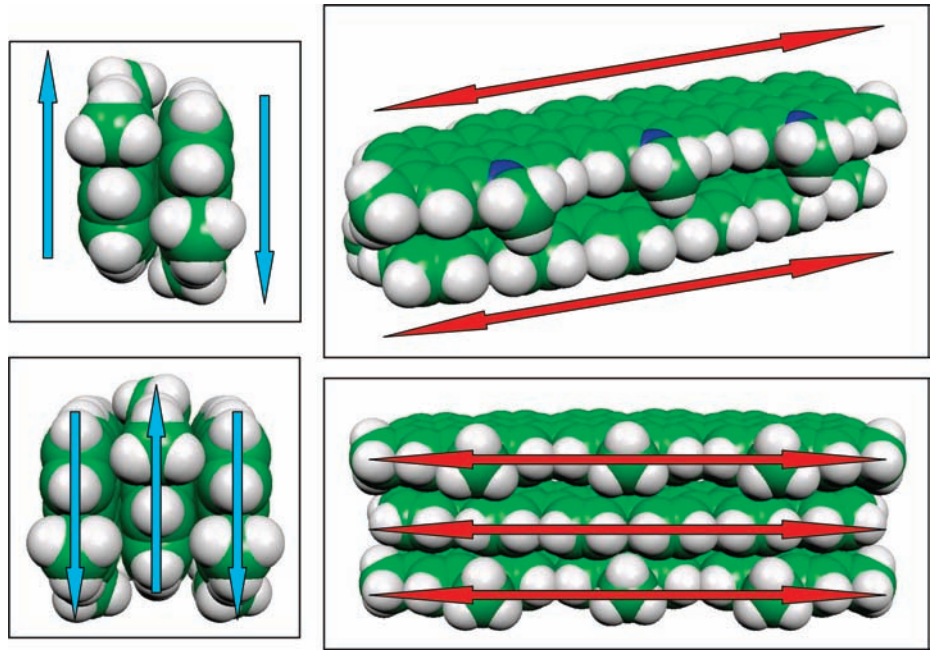

Figure 5. Dimer (top) and trimer (bottom) of TNH as examples of H aggregates. Cyan arrows represent the directions of dipole moments. Red arrows represent the directions of the $S_0 \rightarrow S_1$ transition dipole moments of each molecule.

The observed spectrum of TNH (Figure 3) is similar to those of NP and BNQ, although it shows a strong dependence on substituents. In addition, the relative intensity distribution among the observed bands is markedly concentration dependent (see Figure 6).

Calculations predict a vibronic structure similar to those of NP and BNQ (see Figures S7 and S8) and a remarkable increase in transition dipole moment from NP to TNH (see Tables S1 and S2) as a result of the expanded conjugation along the long molecular axis, which corresponds to the direction of the transition dipole moment (see Figure 5). Thus, the apparent reduction of the observed ε values for **15a**−**c** (Figure 3) must be due to the fact that only a fraction of the TNH monomer is present, while the remaining amount is in the form of aggregate. Indeed, the large computed ground state dipole moment (cyan arrows in Figure 5) induces a remarkable dipole−dipole interaction which justifies the formation of aggregates. Because the transition dipole moment is directed along the long molecular axis, while the ground-state dipole is directed along the short molecular axis, the aggregates are expected to be H type (aggregates showing hypsochromically shifted bands). To model the spectroscopic features associated with aggregates, we considered a dimer and a trimer maximizing the dipole−dipole interaction, oriented as shown in Figure 5 with molecules at a

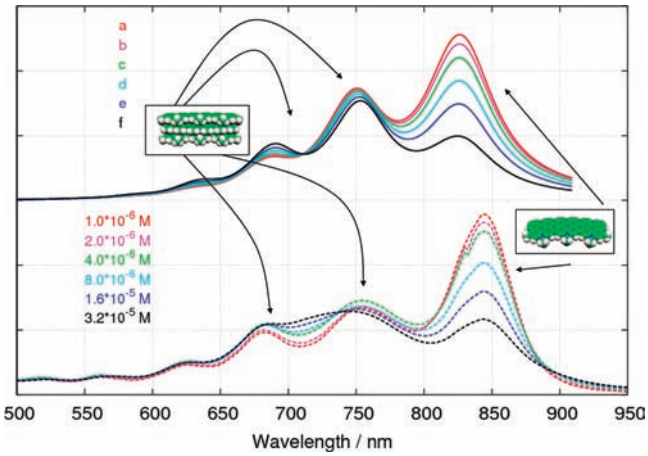

Figure 6. Comparison between observed (bottom) and simulated (top) absorption spectra of TNH. The computed spectra were obtained by superimposing, in different proportions, the spectra of the monomeric and trimeric species with their associated FC structures.

distance of 3.5 Å. Accordingly, the TDDFT computed vertical excitations show a blue shift of the intense excitonic transition (see Table S1 and Figure S9). Assuming, for simplicity, similar vibronic structures for the spectra of the monomer and the aggregate, the computed results are compatible with the intensity dependence of the second, third, and higher bands in the observed absorption spectrum as a function of concentration (see Figure 6). We note in passing that the apparently different aggregation behaviors displayed by **15a**−**c** are not related to the electronic properties of the substituents but rather to their steric hindrance. Indeed, quantum-chemical calculations carried out for **15b**,**c** show similar dipole moments (see Figure S10). However, the large dimensions and the directions of the substituents in **15c** (with respect to the rylene plane) are likely to force the molecules even farther apart, thereby reducing the efficiency of aggregation.

Conclusions

We have reported a highly efficient synthetic methodology toward tri-N-annulated hexarylenes from easily available N-annulated perylenes, which is favored by the oxidative ring fusion driven by DDQ/$Sc(OTf)_3$.

The measured absorption spectra combined with quantum-chemical calculations and modeling of vibronic activities show similar features for NP, BNQ, and TNH with a remarkable activity for frequencies around 1250−1350 cm^{-1} and an increased modulation by low-frequency acoustic modes as the extension of the conjugated framework increases. Because the transition dipole moment associated with the allowed electronic transition is polarized along the long molecular axis, the extension of conjugation is reflected not only in a bathochromic shift of the first transition but also in a strong enhancement of its intensity. At the same time, the large dipole moment (directed along the short molecular axis) favors aggregation of the larger dye (TNH), which is reflected by a decrease of its observed intensity in absorption in combination with a marked concentration dependence of the spectrum, displaying increased intensity on the blue side of the first maximum, consistent with the computed results indicating the formation of H aggregates.

These dyes display remarkably large dipole moments that may favor the formation of highly ordered supramolecular structures, resulting in enhanced charge carrier mobilities. Extension of this synthetic strategy to higher oligomeric graphene nanoribbons as well as further investigation of the structure/properties relationship to tune their electronic, electrostatic, and optic properties are currently underway.

Acknowledgment. For financial support of this research, we thank the National Natural Science Foundation of China (Grant Nos. 50873106 and 20721061), 973 Program, NSFC-DFG joint project TRR61, Chinese Academy of Sciences, and an Italian MIUR grant (PRIN 2008 JKBBK4).

Supporting Information Available: Text, figures, and tables giving experimental details, MS, ^1H NMR, and ^{13}C NMR spectra, computational and modeling details, the optimized structures of **15**−**17**, comparison between computed and experimental absorption spectra of monomeric TNH, active vibrations in electronic spectra, the computed hypsochromic shift for the electronic transition of the aggregates of TNH compared to the monomer, quantum-chemical results for **15b**,**c**, MO energies, absolute energies, and optical and transport gaps for isolated molecules and for small aggregates of TNH, and the largest predicted FC activity of NP, BNQ, and TNH. This material is available free of charge via the Internet at http://pubs.acs.org.

JA100276X